Segmental dynamics of polyethylene-alt-propylene studied by NMR spin echo techniques

A. Lozovoi,[1] C. Mattea,[1] M. Hofmann,[2] K. Saalwaechter,[3] N. Fatkullin,[4] and S. Stapf[1]
[1]*Department of Technical Physics II, Technische Universität Ilmenau, 98684 Ilmenau, Germany*
[2]*Department of Chemistry, Louisiana State University, 70803 Baton Rouge, Louisiana, USA*
[3]*Institut für Physik, Martin-Luther-Universität Halle-Wittenberg, D-06099 Halle (Saale), Germany*
[4]*Institute of Physics, Kazan Federal University, Kazan 420008, Tatarstan, Russia*

(Received 27 December 2016; accepted 15 May 2017; published online 8 June 2017)

Segmental dynamics of a highly entangled melt of linear polyethylene-alt-propylene with a molecular weight of 200 kDa was studied with a novel proton nuclear magnetic resonance (NMR) approach based upon $^1H \rightarrow {}^2H$ isotope dilution as applied to a *solid-echo build-up function* $I^{SE}(t)$, which is constructed from the NMR spin echo signals arising from the Hahn echo (HE) and two variations of the solid-echo pulse sequence. The isotope dilution enables the separation of inter- and intramolecular contributions to this function and allows one to extract the segmental mean-squared displacements in the millisecond time range, which is hardly accessible by other experimental methods. The proposed technique in combination with time-temperature superposition yields information about segmental translation in polyethylene-alt-propylene over 6 decades in time from 10^{-6} s up to 1 s. The time dependence of the mean-squared displacement obtained in this time range clearly shows three regimes of power law with exponents, which are in good agreement with the tube-reptation model predictions for the Rouse model, incoherent reptation and coherent reptation regimes. The results at short times coincide with the fast-field cycling relaxometry and neutron spin echo data, yet, significantly extending the probed time range. Furthermore, the obtained data are verified as well by the use of the dipolar-correlation effect on the Hahn echo, which was developed before by the co-authors. At the same time, the amplitude ratio of the intermolecular part of the proton dynamic dipole-dipole correlation function over the intramolecular part obtained from the experimental data is not in agreement with the predictions of the tube-reptation model for the regimes of incoherent and coherent reptation. *Published by AIP Publishing.* [http://dx.doi.org/10.1063/1.4984265]

INTRODUCTION

Polymers are one of the most widely used industrial materials with the majority of them being operated in the melt state at some point of the manufacturing process. Generally, this type of matter, in comparison to simple liquids, possesses unique properties due to the high length of macromolecules and entanglements occurring between them. Knowledge of the segmental dynamics of macromolecules on the experimental and theoretical level allows one to predict some of the melt's macroscopic characteristics. However, a high number of degrees of freedom in a macromolecule chain leads to the complexity of local motions, covering a wide range of timescales. There is a variety of models addressing this problem in different ways. The most well-established treatment was proposed in a so-called "Rouse model."[1,2] Predictions of the Rouse model hold well for polymer melts with molecular weight $M << M_c$, where M_c is a critical molecular mass above which entanglements become relevant for times $t >> \tau_s$,[3,4] where τ_s is the segmental relaxation time. However, the Rouse model is not able to predict the frequency and molecular weight dependencies of T_1, as well as the diffusion coefficients and segmental mean-squared displacements experimentally observed in the case of entangled polymer melts, i.e., $M > M_c$. One of the most popular theoretical approaches attempting to take into account the topological constraints imposed by entanglements is the tube-reptation model.[5–7] In the frame of this concept, it is assumed that the surrounding of a macromolecule forms a fictitious tube, within which the motion of the chain is constrained, thus introducing an additional source of intermolecular forces in a polymer melt in comparison with the Rouse model. In this scenario, the whole time range of segmental dynamics can be separated into four regimes, characterized by different time limits. At times $\tau_s << t << \tau_e$ (τ_e is the entanglement time) the chain senses no constraints, and its dynamics follows the Rouse model. The second regime, which can be named incoherent reptation, stands for the slower dynamics determined by the motions of the chain in a tube at times $\tau_e << t << \tau_R$, where $\tau_R = \tau_s N^2$ is the longest Rouse mode relaxation time. In this regime, a single chain already reptates inside the tube, but different parts of it move independently from each other and the effects of the contour length fluctuations are playing an important role. At longer times, the effect of the coherent reptation takes place, when the chain coherently moves along the tube in the time interval $\tau_R << t << \tau_d$, where τ_d is known as a disengagement time. At times $t >> \tau_d$, the chain leaves the tube and the diffusion eventually becomes "normal." The characteristic time and molecular weight dependencies for each regime resulting from the tube-reptation model are summarized below:[3,5–8,14]

- $\tau_s << \left(t, \frac{1}{\omega}\right) << \tau_e \quad \langle r^2(t)\rangle \propto M^0 t^{0.5} \quad \frac{1}{T_1} \propto M^0 \ln(1/\omega\tau_s),$
- $\tau_e << \left(t, \frac{1}{\omega}\right) << \tau_R \quad \langle r^2(t)\rangle \propto M^0 t^{0.25} \quad \frac{1}{T_1} \propto M^0 \omega^{-\frac{3}{4}},$
- $\tau_R << \left(t, \frac{1}{\omega}\right) << \tau_d \quad \langle r^2(t)\rangle \propto M^{-0.5} t^{0.5} \quad \frac{1}{T_1} \propto M^{\frac{1}{2}} \omega^{-\frac{1}{2}},$
- $\tau_d << \left(t, \frac{1}{\omega}\right) \quad \langle r^2(t)\rangle \propto M^{-2} t^{1} \quad \frac{1}{T_1} \propto M^2 \omega^0.$

A number of other theoretical models describing the segmental dynamics in polymer melts has been developed over the years, such as renormalized Rouse models[9,10] and the mode-mode coupling model.[11] Nevertheless, none of the mentioned models is able to explain all the experimental results obtained in polymer melts. Therefore, the study of the segmental dynamics in polymers at different time scales is still of high importance for discriminating between different model predictions.

Nuclear magnetic resonance (NMR) based methods have always been widely used for the study of polymer melts,[12–14] specifically ^{1}H NMR, since polymers contain a large number of ^{1}H nuclei. For proton spins, $I = \frac{1}{2}$, the detectable relaxation of the nuclear magnetization is determined by the dipole-dipole interactions,[12] which in turn are modulated by the molecular motions. In Refs. 15–17, it was theoretically predicted for the first time and also experimentally proven with the use of a fast field-cycling (FFC) relaxometry technique that intra- and inter-molecular contributions to dipole-dipole interactions in polymer melts can be isolated from each other via isotopic dilution and studied separately. This finding gave a new rise to fundamental NMR investigations of polymer melt segmental dynamics with FFC methods,[18–24] which, with the help of frequency-temperature superposition combined with field-gradient (FG) NMR experiments, are describing processes in melts in a very wide time range.[25] However, both field-cycling relaxometry (FC) as well as FG NMR techniques have certain limitations, frequently imposed by the NMR hardware. Conventional FFC relaxometers are not able to directly probe frequencies lower than ~10 kHz (corresponding to times longer than ~100 μs). A number of works performed on a dedicated home-built FFC machine, allowing ultra-low magnetic field measurements, were presented recently.[22,23] In this case, one has to take into consideration a possible non-exponentiality of the longitudinal magnetization decay due to the violation of the Redfield limit and the presence of the local magnetic fields.[12] On the other hand, the FG methods are limited by the maximum achievable gradient strength necessary for probing the slow dynamics of a chain and effects of spin-diffusion,[26] usually corresponding to the smallest accessible mean-squared displacements (MSD) of about 200 Å.

Another powerful and widely used tool for the investigation of the segmental dynamics in polymers is quasi-elastic neutron scattering (QENS) and neutron spin echo (NSE).[27–29]

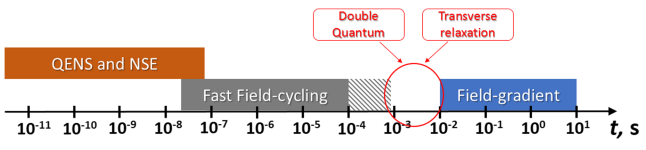

FIG. 1. Time scale of a highly entangled polymer melt's segmental dynamics accessible by different techniques. The hatched part of FFC rectangle represents the time range covered with the help of ultra-low field experiments.

The longest times and largest displacements available for these methods are dictated by the lowest value of the scattering wave vector k and the maximum temperature the polymer can withstand before the onset of degradation. Typically, this corresponds to displacements in the order of 10 Å and times around 10 ns (in the best case 100 ns and 30 Å).

The schematic representation of the time ranges covered by different NMR techniques and neutron scattering is shown in Fig. 1 for the better illustration.

One can see that the interval from 100 μs to 10 ms is either not directly covered or hardly accessible by the discussed techniques (at least demanding a particularly sophisticated hardware). This gap can be studied with the use of double-quantum (DQ) coherence excitation,[30–34] which requires in its most quantitative incarnation the application of a sophisticated radio frequency (RF) pulse sequence. Alternatively, methods based on treating the transverse magnetization decay can be used for the same purpose, employing such experimental techniques as a simple free induction decay (FID), the Hahn echo (HE), the dipolar-correlation effect (DCE) or the solid echo (SE).[35–40] Recently a new method, based on the DCE on the Hahn echo decay, has been developed and applied to obtain the segmental mean-squared displacements in a highly entangled polybutadiene melt,[41] with results that are in good agreement with the results provided by FFC NMR. In this work, we present a novel complementary method for investigating the translational motion of segments in polymer melts. The experimental technique relies on the construction of a build-up function which is essentially identical to that of earlier approaches described in Refs. 42–46. However, in the cited works the theoretical analyses were restricted to a spin-pair approximation, i.e., absolutely ignoring intermolecular magnetic dipole-dipole interactions. The method proposed in the present study is based on a formalism which considers all the spins in the system. It is applied to the evaluation of the Hahn-echo and the solid-echo NMR signals, and covers the above mentioned gap in the experimentally accessible times in the millisecond range.

THEORY

In order to extract information about the time dependence of the proton dipole-dipole correlation function and segmental mean-squared displacements in a polymer melt, a special function should be considered, which is constructed from signals given by three different spin echo experiments:

- S_1 - $\left(\hat{P}_x^{\pi/2} - \tau - \hat{P}_y^{\pi/2}\right)$, known as *solid echo*,
- S_2 - $\left(\hat{P}_x^{\pi/2} - \tau - \hat{P}_x^{\pi/2}\right)$,
- S_3 - $\left(\hat{P}_x^{\pi/2} - \tau - \hat{P}_x^{\pi}\right)$, known as *Hahn echo*,

where $\hat{P}_\alpha^\theta$ is an operator, rotating the spin system by the angle θ about axis α. This function is named the *solid-echo build-up*

function and is defined by the following equation:

$$I^{SE}(t) \equiv \frac{S_1(t) + S_2(t) - S_3(t)}{S_1(t) + S_2(t)}. \quad (1)$$

In this expression, $t = 2\tau$ is the time moment at which the spin echo is observed and τ is the interval between two RF pulses. For any exponential relaxation decay, the solid-echo build-up function equals zero, which means that any possible contributions from the mobile fractions are removed. It will be shown that the initial rise of this function contains additive contributions from intra- and intermolecular dipole-dipole interactions, with the latter comprising the information about translational motion of segments. Note that for a two-spin system the introduced function $I^{SE}(t)$ is analogous to the $\Gamma(t)$ function described in Refs. 42 and 43 and $\beta(2\tau; \tau)$ function discussed in Refs. 44 and 45, see also similar approaches in Ref. 46 and the literature cited therein.

Following the mathematical derivation presented in the Appendix, one can obtain with help of modified Anderson-Weiss approximation the expression for the $I^{SE}(t)$ for spins $I = \frac{1}{2}$,

$$I^{SE}(t) = 1 - \frac{\sum\limits_k \exp\left\{-\frac{1}{8}\sum\limits_m \left\langle \left(\tilde{\varphi}^d_{km}(\tau) + \varphi^d_{km}(\tau)\right)^2 \right\rangle\right\}}{\sum\limits_k \exp\left\{-\frac{1}{8}\sum\limits_m \left\langle \left(\tilde{\varphi}^d_{km}(\tau) - \varphi^d_{km}(\tau)\right)\right\rangle\right\}}, \quad (2)$$

where

$$\varphi^d_{km}(\tau) = \frac{3\gamma^2\hbar}{2}\int\limits_0^\tau dt_1 \frac{1 - 3\cos^2(\theta_{km}(t_1))}{r^3_{km}(t_1)} P^{fl}_{km}(t_1), \quad (3)$$

$$\tilde{\varphi}^d_{km}(t-\tau) = \frac{3\gamma^2\hbar}{2}\int\limits_\tau^t dt_1 \frac{1 - 3\cos^2(\theta_{km}(t_1))}{r^3_{km}(t_1)} P^{fl}_{km}(t_1). \quad (4)$$

The quantities $\varphi^d_{kl}(\tau)$ and $\tilde{\varphi}^d_{km}(t-\tau)$ are related to the motion of proton spins in local dipolar fields after the first and the second RF pulses, respectively, and contain information about polymer segments dynamics through the time dependence of the factors $\frac{1-3\cos^2(\theta_{km}(t_1))}{r^3_{km}(t_1)}$ inside the integrals at the right-hand sides of expressions (3) and (4). The bracket $\langle \ldots \rangle$ denotes the equilibrium averaging over lattice variables.

For the situations when all the spins are equivalent, i.e., terms inside the sums in the expression (2) do not depend on k, this can be simplified to

$$I^{SE}(t) = 1 - \frac{1}{N_s}\sum_k \exp\left\{-\frac{1}{2}\sum_m \left\langle \tilde{\varphi}^d_{km}(\tau)\cdot\varphi^d_{km}(\tau)\right\rangle\right\}$$
$$= 1 - \exp\left\{-\frac{1}{2N_s}\sum_{k;m}\left\langle \tilde{\varphi}^d_{km}(\tau)\cdot\varphi^d_{km}(\tau)\right\rangle\right\}, \quad (5)$$

where N_s is the total number of spins in the system with the resonance frequency ω_0. Note that in the many-spins system the function $I^{SE}(t)$ is similar to the so-called double-quantum build-up function $I_{nDQ}(\tau_{DQ})$, which was derived in Ref. 34; the two functions differ only in a numerical factor.

The main approximation made in the course of the derivation of Eq. (5) is the modified Anderson-Weiss approximation first formulated in Ref. 35. It is exact for times $t << T_2^{eff}$, where T_2^{eff} is the time, at which a transverse magnetization decays to e^{-1} of its initial value, and takes into account (at variance with the ordinary Anderson-Weiss approximation) flip-flop processes causing spin-diffusion for times $t > T_2^{eff}$. It is clearly observed that all the obtained expressions contain both intra- and inter-molecular magnetic dipole-dipole interactions between proton spins.

At times $t < T_2^{eff}$ the argument in the exponential in (5) is small, thus enabling one to decompose this expression into a Taylor series. Keeping only the terms quadratic in phase yields

$$I^{SE}(t) = \frac{1}{2N_s}\sum_{k;m}\left\langle \tilde{\varphi}^d_{km}(\tau)\cdot\varphi^d_{km}(\tau)\right\rangle + \ldots. \quad (6)$$

Then using the expressions (3)–(5) and employing the translational invariance of the time-dependent correlation functions, (6) can be rewritten as follows:

$$I^{SE}(t) = \frac{9}{8}\gamma^4\hbar^2\int\limits_0^\tau (\tau - t_1)\left\{A^d_0(\tau + t_1) + A^d_0(\tau - t_1)\right\} dt_1 + \ldots, \quad (7)$$

where

$$A^d_0(t) = \frac{1}{N_s}\sum_{k,m}\left\langle \frac{1 - 3\cos(\theta_{km}(t))}{r^3_{km}(t)}\cdot\frac{1 - 3\cos(\theta_{km}(0))}{r^3_{km}(0)}\right\rangle. \quad (8)$$

The time dependent total dipole-dipole correlation function $A^d_0(t)$ for polymer melts was analyzed in details earlier.[35] It can be separated into a sum of intermolecular and intramolecular parts, corresponding to the contributions from protons from the different and the same macromolecules, respectively,

$$A^d_0(t) = A^{d;inter}_0(t) + A^{d;intra}_0(t). \quad (9)$$

The intermolecular contribution for times much longer than the segmental relaxation time $t >> \tau_s$ is connected with the relative mean-squared displacement of proton spins from different macromolecules $\langle \tilde{r}^2(t)\rangle$ by the following expression:

$$A^{d;inter}_0(t) = \sqrt{\frac{2}{3\pi}}\frac{16\pi}{5}\frac{n_s}{\langle \tilde{r}^2(t)\rangle^{3/2}}, \quad (10)$$

where n_s is the volume density of protons in the system. Considering (9), the experimentally measurable function $I^{SE}(t)$ can also be represented as the sum of intramolecular and intermolecular contributions,

$$I^{SE}(t) = I^{SE;intra}(t) + I^{SE;inter}(t). \quad (11)$$

With the use of relation (10), it is possible to demonstrate that the intermolecular part of the build-up function is connected in a rather simple way with the relative mean-squared displacements of polymer segments from different macromolecules:

$$I^{SE;inter}(t) = \frac{18\pi}{5}\sqrt{\frac{2}{3\pi}}\gamma^4\hbar^2 n_s\int\limits_0^\tau (\tau - t_1)\left\{\frac{1}{\langle \tilde{r}^2(\tau + t_1)\rangle^{3/2}} + \frac{1}{\langle \tilde{r}^2(\tau - t_1)\rangle^{3/2}}\right\} dt_1 + \ldots. \quad (12)$$

In the case when the relative mean-squared displacement of polymer segments from different macromolecules can be

described by a time independent exponent α, i.e., $\langle \tilde{r}^2(t) \rangle = A \cdot t^{\alpha}$, integration of the right-hand side of expression (12) can be performed exactly with the assumption that $\alpha < 2/3$, yielding

$$I^{SE;inter}(t) = \frac{18\pi}{5} f(\alpha) \sqrt{\frac{2}{3\pi}} \gamma^4 \hbar^2 n_s \frac{t^2}{\langle \tilde{r}^2(t) \rangle^{3/2}} + ..., \quad (13)$$

where

$$f(\alpha) = \frac{2^{\frac{3\alpha}{2}} \left(2^{1-\frac{3\alpha}{2}} - 1\right)}{4 \left(1 - \frac{3\alpha}{2}\right) \left(1 - \frac{3\alpha}{4}\right)}. \quad (14)$$

From Eq. (13), one can obtain the relative mean-squared displacement of polymer segments from different polymer chains,

$$\left\langle \tilde{r}^2(t) \right\rangle = \left(\frac{18\pi}{5} f(\alpha) \sqrt{\frac{2}{3\pi}} \gamma^4 \hbar^2 n_s \frac{t^2}{I^{SE;inter}(t)} \right)^{\frac{2}{3}}. \quad (15)$$

Note that the characteristic flip-flop time is considerably longer than the spin-spin relaxation time $\tau_{fl} \approx \left(\frac{9}{2}\right)^{\frac{2}{4-3\alpha}} T_2^{eff} > 2T_2^{eff}$.[35] Then for times $\tau < \tau_{fl} \approx \left(\frac{9}{2}\right)^{\frac{2}{4-3\alpha}} T_2^{eff}$, expression (5) can be rewritten as

$$I^{SE;inter}(t) = 1 - \exp\left\{ -\frac{18\pi}{5} \sqrt{\frac{2}{3\pi}} \gamma^4 \hbar^2 n_s \int_0^{\tau} (\tau - t_1) \times \left\{ \frac{1}{\langle \tilde{r}^2(\tau + t_1) \rangle^{3/2}} + \frac{1}{\langle \tilde{r}^2(\tau - t_1) \rangle^{3/2}} \right\} dt_1 + ... \right\}. \quad (16)$$

The relative mean-squared displacement of polymer segments from different macromolecules for time-independent exponent α can then be calculated using the following relation:

$$\left\langle \tilde{r}^2(t) \right\rangle = \left(\frac{18\pi}{5} f(\alpha) \sqrt{\frac{2}{3\pi}} \gamma^4 \hbar^2 n_s \frac{t^2}{\ln\left(\frac{1}{1 - I^{SE;inter}(t)}\right)} \right)^{\frac{2}{3}}. \quad (17)$$

The experimental results processed using this expression are going to be compared with the results calculated with the help of another method described recently in Ref. 41. It implies the construction of the dipolar-correlation build-up function, correlating the Hahn echo signals at time moments $\frac{t}{2}$ and t: $I^{DC}(t) = 1 - \frac{S^{HE}(t) S^{HE}(0)}{\left(S^{HE}\left(\frac{t}{2}\right)\right)^2}$, where $S^{HE}(t)$ is the Hahn echo signal at the time moment $t = 2\tau$. Then the MSD can be obtained from the intermolecular part of $I^{DC}(t)$,

$$\left\langle \tilde{r}^2(t) \right\rangle = \left(\frac{9\pi}{5} f(\alpha) \sqrt{\frac{2}{3\pi}} \gamma^4 \hbar^2 n_s \frac{t^2}{\ln\left(\frac{1}{1 - I^{DC;inter}(t)}\right)} \right)^{\frac{2}{3}}. \quad (18)$$

EXPERIMENT

Poly(ethylene-alt-propylene) (PEP) with a narrow molar mass (M) distribution (Mn/Mw < 1.06) was synthesized from poly(isoprene) via hydrogenation[47] and kindly provided by D. Richter (Forschungszentrum Jülich, Germany). The polymer combines a very simple structure, a low glass transition temperature of $T_g = 206$ K,[24] and only a weak tendency to crystallize. Two samples were prepared: one of them represents fully protonated PEP with a molar mass of M = 200 kDa. The second sample is an isotopic mixture composed of fully protonated and fully deuterated PEP of the same molecular weight 200 kDa, with weight fractions of 10% ^{1}H and 90% ^{2}H, respectively, blended according to the procedure described in Ref. 22. The concentration was controlled through weighing. For the NMR measurements, the samples were filled into standard 5 mm NMR tubes and then degassed under vacuum at around 330 K for at least 48 h to remove paramagnetic oxygen. Both samples were in a highly entangled state due to the molecular weight of 200 kDa significantly exceeding the critical mass of PEP, $M_c \sim 2$kDa;[48] therefore, the anomalous segmental diffusion regime is expected in a broad range of time, representing the point of interest for the present work. Transverse NMR relaxation experiments were performed in a broad temperature range T = 283 K–440 K using three different NMR spectrometers. The measurements at temperatures T = 283 K–338 K were carried out on a Minispec mq40 (Bruker, ^{1}H 40 MHz) in the University of Ilmenau. The intermediate temperature range T = 338 K–400 K was covered on the Minispec mq20 (Bruker, ^{1}H 20 MHz) in the University of Halle, Germany. Finally, high temperatures above 400 K were covered with the use of a homemade relaxometer based on a Halbach design magnet[51] operating at a ^{1}H frequency of 17 MHz in Ilmenau. The results of all the measurements at different T were treated in the same way, since the analysis of the data based on the formalism developed before is independent from the Larmor frequency. In order to calculate the solid-echo build-up function $I^{SE}(t)$, one needs to obtain signals S_1, S_2, and S_3 resulting from three different pulse sequences $\left(\hat{P}_x^{\pi/2} - \tau - \hat{P}_y^{\pi/2}\right)$, $\left(\hat{P}_x^{-\pi/2} - \tau - \hat{P}_x^{-\pi/2}\right)$, and $\left(\hat{P}_x^{-\pi/2} - \tau - \hat{P}_x^{\pi}\right)$, as was discussed earlier. In principle, the numerator of $I^{SE}(t)$, $S_1 + S_2 - S_3$, can be obtained in one single experiment, using the pulse sequence $\left(\hat{P}_x^{\pi/2} - \tau - \hat{P}_{k_1}^{\pi/2} \hat{P}_{k_2}^{\pi/4} \hat{P}_{k_3}^{\pi/4}\right)$ with proper phase cycling for k_1, k_2, k_3 so that the $\pi/4$ RF pulses are either in phase (Hahn echo S_3) or cancel each other (S_1 or S_2). However, this type of experiments demands a high homogeneity of the RF field, otherwise artifacts connected with a non-perfect angle of a magnetization flip following the RF pulse can appear. In this work, signals S_3 and $S_{12} = S_1 + S_2$ (with the use of phase cycling) were measured separately and were then combined in order to obtain $I^{SE}(t) = \frac{S_{12}(t) - S_3(t)}{S_{12}(t)}$. As an example, in Fig. 2 the solid-echo build-up function I^{SE} is plotted as a function of time $t = 2\tau$ for the fully protonated and the diluted sample at $T = 333$ K.

The representation of these data into the relative mean-squared displacements according to Eq. (17) is valid only for times $t < T_2^{eff}$. Thus, the area of the curves which was not used for analysis is marked on the plot, corresponding to T_2^{eff} of the protonated sample, as it is always lower than T_2^{eff} of the diluted one, due to the almost full elimination of the intermolecular proton dipole-dipole interactions in the latter. The intermolecular part of the build-up function $I^{SE;inter}(t)$, which is necessary for obtaining MSD with the use of (17), can be extracted from these data via extrapolation to zero proton

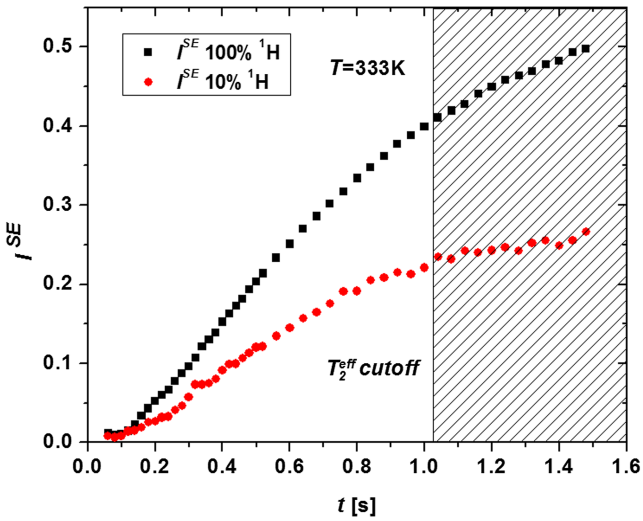

FIG. 2. Proton solid-echo build-up function I^{SE} as a function of time for the protonated (100% ^{1}H) and diluted (10% ^{1}H) PEP 200k. The vertical line marks the T_2^{eff} characteristic time of a transverse magnetization decay for the protonated sample.

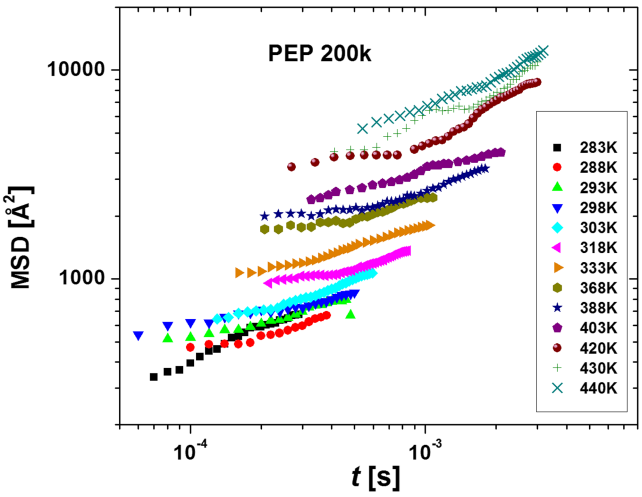

FIG. 3. Segmental mean-squared displacements $\langle r^2(t)\rangle$ of PEP 200k for different temperatures.

content in the polymer sample,

$$I^{SE;inter}(t) = 1 - \left(\frac{1 - I_\upsilon^{SE}(t)}{1 - I_p^{SE}(t)}\right)^{-\frac{1}{1-\upsilon}}. \quad (19)$$

Here, υ is the proton concentration in the diluted sample and $I_p^{SE}(t)$ and $I_\upsilon^{SE}(t)$ are solid-echo build-up functions of the protonated and the diluted samples, respectively.

Note that Eq. (17) only yields the relative MSD $\langle \tilde{r}^2(t)\rangle$ of polymer segments from different chains. At the present state of polymer dynamics theory, a detailed model connecting the relative mean-squared displacement $\langle \tilde{r}^2(t)\rangle$ of two polymer segments with the absolute mean-squared displacement of individual polymer segments $\langle r^2(t)\rangle$ over the whole time range has not been formulated. However, it is reasonable to expect that they are connected in the following way: $\langle \tilde{r}^2(t)\rangle = \tilde{\alpha}\langle r^2(t)\rangle$, where $\tilde{\alpha} \le 2$, depending on the degree of correlation of segmental motions. In the case when motions of polymer chains are not correlated $\tilde{\alpha} = 2$, which certainly takes place in the normal diffusion regime, whereas $\tilde{\alpha} = 0$ in the case when segmental motions are completely correlated, i.e., segments are rigidly bonded. Further on, it is assumed that $\tilde{\alpha} = 2$ holds over the whole time range covered by the experiments, leading to the simple relation $\langle \tilde{r}^2(t)\rangle = 2\langle r^2(t)\rangle$. In Fig. 3, the segmental mean-squared displacement $\langle r^2(t)\rangle$ at different temperatures T = 283 K–440 K is plotted. It was calculated from the solid-echo build-up functions I^{SE} with the use of Eq. (17).

The long-time limitations of validity of the curves for each temperature are connected with the value of T_2^{eff}, which is increasing with T. On the other hand, the short-time limit is determined by the difference between the values of I_p^{SE} and I_υ^{SE}, which is becoming too small, leading to a high uncertainty of the calculated $I^{SE;\,inter}$ and, consequently, of $\langle r^2(t)\rangle$. In addition to that, it is necessary to mention the problem of calculation of $f(\alpha)$, given by (14) and appearing in (17), as it depends on the *a priori* unknown power-law exponent of the MSD time dependence's power law. Taking into account the fact that α in polymer melts is always in the range $0.2 \le \alpha \le 0.5$, the maximum range of $f(\alpha)$ and, thus, of the numerical coefficient for MSD in (17) is $\left(\frac{f(0.5)}{f(0.2)}\right)^{\frac{2}{3}} \cong 1.36$. A more careful mathematical treatment of that problem is necessary, whereas in this work the simple model of a linear change of α during the transitions was assumed.

In order to illustrate the actual interval of the measured displacements in time, the time-temperature superposition (TTS) principle was applied. It relies on the assumption that no phase and no glass transition takes places within the probed temperature range, and that the temperature dependence of the Kuhn segment length is negligible. The temperature dependent coefficients applied for the horizontal (i.e. time) shift of MSD curves in Fig. 3 relative to the reference temperature were taken from the segmental relaxation time temperature dependence data $\tau_s(T)$ obtained by shear rheology, dielectric spectroscopy, and FFC NMR, presented in Ref. 23 and shown in Fig. 6 as well. The reference temperature was set to be 333 K and results were compared with the MSD of PEP with M = 80 kDa measured by means of neutron spin echo spectroscopy carried out by Wischnewsky *et al.* at the temperature of 492 K.[28] In order to perform such a comparison the extrapolation of the $\tau_s(T)$ to 492 K was done and the value of τ_s obtained in this way (marked in Fig. 6) was used for the temperature shift of the NSE data. The result of this superposition yields a master curve shown in Fig. 4.

One can see that data obtained by the combination of NMR spin echoes coincides well with NSE data in the time interval $t \approx 10^{-6}$–10^{-5} s and extends significantly the probed time range of the segmental mean-squared displacements up to ≈1 s at $T = 333$ K. Three power-law regimes are revealed. Two transition times were estimated from the intersections of the power laws: $\tau_e \approx 4.6$ μs, corresponding to the transition between the Rouse (I, $t < \tau_e$) and the incoherent reptation (II, $\tau_e < t < \tau_R$) regime, and $\tau_R \approx 47$ ms, marking the transition between incoherent reptation (II) and coherent reptation (III, $t > \tau_R$)

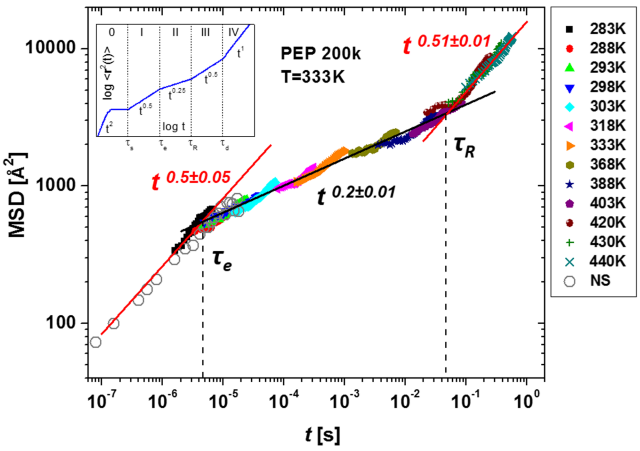

FIG. 4. PEP 200k MSD time dependence obtained via time-temperature superposition of the curves in Fig. 3 and MSD of PEP 80k measured by neutron spin echo (NSE) spectroscopy.[28] Three different power-law regimes are revealed with exponents as indicated. The crossover times τ_e and τ_R are determined from the intersections of the power laws. The inset shows the predictions of the tube-reptation model for the MSD time dependence.

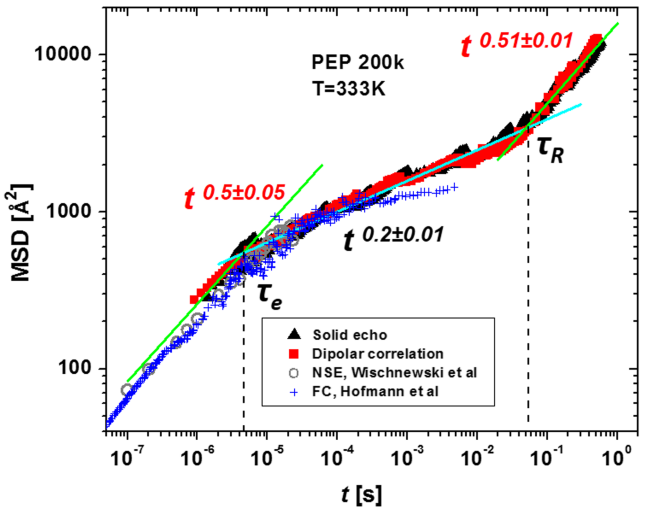

FIG. 5. PEP 200k MSD time dependence obtained through $I^{SE;inter}$ (the solid echo formalism) and $I^{DC;inter}$ (the dipolar correlation effect) compared with FC data in PEP 200k[24] and MSD of PEP 80k measured with the use of NSE.[28]

regimes in the frames of the tube-reptation model. It is noted that to the best of the authors' knowledge, the latter transition in PEP 200k was observed for the first time.

The exponents of the power laws in regimes (I) $\alpha = 0.5 \pm 0.05$ and (III) $\alpha = 0.51 \pm 0.01$, respectively, are in good agreement with the values predicted by the tube-reptation model ($\alpha = 0.5$), whereas in regime (II) the observed exponent $\alpha = 0.2 \pm 0.01$ is lower than the theoretical value of $\alpha = 0.25$. Model prediction for the ratio between τ_R and τ_e for the case of PEP is $\frac{\tau_R}{\tau_e} = \frac{N^2}{N_e^2} \cong 8\,000$, where N_e is a number of Kuhn segments corresponding to one entanglement. The data displayed in Fig. 4 yields the value $\frac{\tau_R}{\tau_e} \approx 10\,000$, which is remarkably close to the theoretical predicted one.

With these results, it is possible to estimate the characteristic tube diameter d_t of polyethylene-alt-propylene using the value of τ_e: $\langle r^2(\tau_e)\rangle^{\frac{1}{2}} = \sqrt{\frac{2}{\pi^{\frac{3}{2}}}} d_t$,[8] resulting in $d_t = \sqrt{\frac{\pi^{\frac{3}{2}}}{2}} \langle r^2(\tau_e)\rangle^{\frac{1}{2}} \approx 3.9$ nm, which is in good agreement with the calculated value 4.88 nm and the NSE data yielding 4 nm from Ref. 48.

In Ref. 23, the same polymer PEP 200k was studied with field-cycling relaxometry and the values of $\alpha \approx 0.5$ for regime I and $\alpha \approx 0.2$ in the beginning of regime II were obtained, as well as the tube diameter of 4.6 nm. In Fig. 5, the MSD obtained from NMR spin echo presented in Fig. 3 is compared with the FC relaxometry and NSE data, and with the results from the method based on the dipolar correlation effect on the Hahn echo (DC), using expression (18). For the latter, again the principle of time-temperature superposition was applied for constructing a master curve using the same temperature shift factors as before.

Exceeding the time range of NSE spectroscopy and FFC relaxometry, the presented spin echo method, as well as the dipolar correlation based method, is able to reach regime III of the tube-reptation model. Dipolar correlation data clearly yields 3 regimes of time-dependent segmental MSD with exponents close to the ones observed with the use of $I^{SE;inter}$. The difference of absolute values of MSD between these two methods is satisfactory; the tube diameter calculated from DC data is slightly higher than calculated before $d_t \approx 4.2$ nm.

In addition to that, it should be taken into account that the $I^{SE;inter}$ build-up function has an amplitude two times higher than that of the $I^{DC;inter}$ function, which can be seen from the comparison of (16) and the analogous expression for $I^{DC;inter}$ in Ref. 41. This leads to a better signal-to-noise ratio of the formalism presented in this work than that of the dipolar correlation based method. At the same time, the latter is technically simpler, demanding only performing a Hahn echo experiment. On the contrary, for the construction of the I^{SE} function, a series of double pulse experiments with perfectly tuned receiver phase and RF pulses of a high-quality is necessary.

In Fig. 6, the temperature dependencies of all the characteristic time constants of the tube-reptation model in PEP are presented: segmental relaxation time τ_s, entanglement time τ_e, Rouse relaxation time τ_R, and disengagement relaxation time τ_d. The graph is based on Fig. 7 from Ref. 24 with the addition of the data obtained in the present work by the spin echo method. Values of $\tau_s(T)$ are provided by ^{1}H FC NMR, shear-stress rheology,[24] dielectric spectroscopy, and solid-state ^{2}H NMR[49] for different molecular weights of PEP, since τ_s is weight independent. $\tau_s(T)$ data are interpolated by a four-parameter function[50] and this function is vertically shifted to intersect τ_e, τ_R, and τ_d values. The presented values of the entanglement time τ_e for PEP 200k are obtained with the use of NSE,[28] ^{1}H FC NMR,[24] and the spin echo method, described in this work. It is clearly seen that τ_e provided by the spin echo method for T = 333 K is in good agreement with the other two experimental values. Furthermore, the spin echo method is the only one providing the value of the Rouse relaxation time τ_R for PEP 200k. In addition to this, temperature dependence of the terminal relaxation time for PEP 200k $\tau_d(T)$ obtained with the use of shear-stress rheology[24] is shown for the complete illustration of the relaxation times map in PEP.

Another important analysis, which can be performed in the frame of the presented formalism, is the investigation of the relative contributions of the intermolecular and

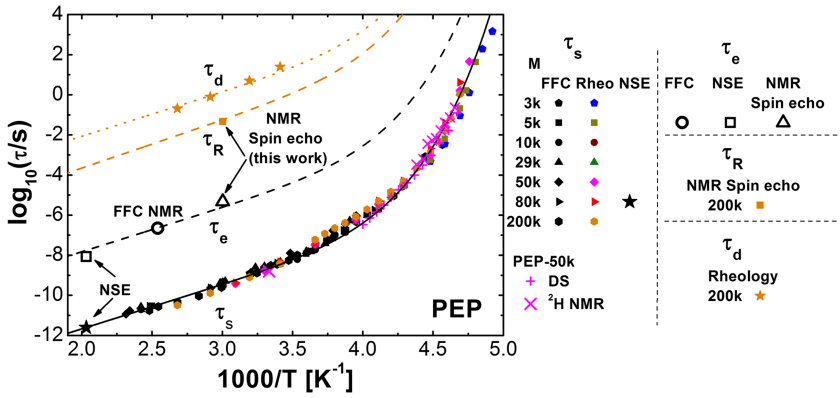

FIG. 6. Relaxation map of PEP: τ_s (T) for different M determined by ^{1}H FC NMR (black closed symbols), shear-stress rheology (colored closed points),[24] NSE (extrapolated), dielectric spectroscopy (unpublished data), and solid-state ^{2}H NMR (crosses).[49] τ_e (T) values for PEP 200k are obtained by ^{1}H FC NMR,[24] NSE,[28] and the spin echo method presented in this work. The value of τ_R at T = 333K for PEP 200k is provided only by the spin echo method. τ_d (T) is measured with the use of shear-stress rheology.[24] τ_s (T) data are interpolated by a four-parameter function (solid black line),[50] and this function is vertically shifted to intersect τ_e, τ_R, and τ_d values (dashed lines).

intramolecular interactions to the total dipole-dipole correlation function. These contributions A^{inter} (translational) and A^{intra} (reorientational) are contained in the exponent of the normalized Hahn echo signal[35] and their ratio can be extracted in the following way:

$$\frac{A^{\text{inter}}}{A^{\text{intra}}} = \frac{L_p(t) - L_v(t)}{L_v(t) - vL_p(t)}. \tag{20}$$

In this expression, $L_p(t)$ and $L_v(t)$ are logarithms of the normalized Hahn echo signals of protonated and diluted samples, respectively. It is noted that the ratio $\frac{A^{\text{inter}}}{A^{\text{intra}}}$ is, by nature of its construction, not normalized for exponential transverse relaxation contributions corresponding to the highly mobile fractions, which may well differ for the inter- and intramolecular contributions. Apart from that, the additivity assumption inherent to the "single-point" extrapolation of A^{inter} used in this work will have to be checked by means of an isotope dilution series, which was beyond the current scope.

It is known[52] that the model prediction for the ratio of the intermolecular part of the dipole-dipole correlation function over the intramolecular part in the case of isotropic dynamics, when the segment displacements are not correlated with the initial conformation of a chain, is $\frac{A^{\text{inter}}}{A^{\text{intra}}} \propto \langle r^2(t)\rangle^{\frac{1}{2}}$. On the contrary, in the case of anisotropic segmental motions, as for instance, within regime II and III in the frame of the tube-reptation model at times $\tau_e < t < \tau_R$, theory yields $\frac{A^{\text{inter}}}{A^{\text{intra}}} \propto \langle r^2(t)\rangle^{-\frac{1}{2}}$. Therefore, calculating and plotting $\frac{A^{\text{inter}}}{A^{\text{intra}}}$ against the root mean-squared displacement $\langle r^2(t)\rangle^{\frac{1}{2}}$ (RMSD) allows one to discriminate between fundamentally different models. This graph is presented in Fig. 7(a) along with the dependence predicted by the tube-reptation model.

The exponent of a $\frac{A^{\text{inter}}}{A^{\text{intra}}}$ dependence on RMSD in regime I ($\tau_s < t < \tau_e$) is 1.28 ± 0.08, which is sufficiently close to the theoretical prediction for isotropic models. Interestingly, the behavior of $\frac{A^{\text{inter}}}{A^{\text{intra}}}$ in regimes II and III is completely different from what follows from the model prediction: here the ratio grows as a function of RMSD with the exponent of the power law 0.47 ± 0.02 in regime II, tending to reach a plateau in regime III. Calculation of the reorientational and translational dipole-dipole correlation functions for PEP 200k employing FFC relaxometry data was as well performed in Ref. 24 for regime I and the beginning of regime II. The comparison of these data to the results obtained in this work is shown in Fig. 7(b). Here, the ratio $\frac{A^{\text{inter}}}{A^{\text{intra}}}$ is plotted as a function of the normalized time t/τ_e, showing essentially different behavior of the data provided by different methods for times $t/\tau_e = 10^{-1} - 10^3$. This apparent contradiction between the results of the present work and FC relaxometry data needs to be further investigated. Preliminary explanation of this phenomenon can rely

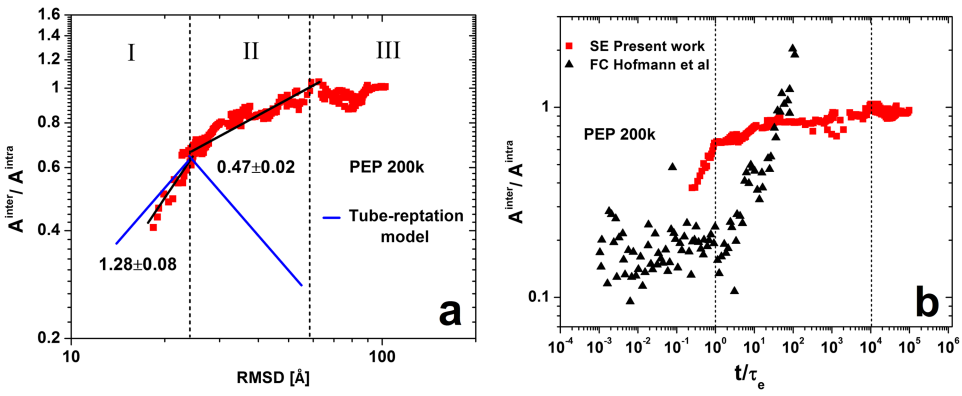

FIG. 7. (a) Ratio of the intermolecular dipole-dipole interactions contribution to the total dipole-dipole correlation function over the intramolecular contribution in PEP 200k as a function of the root mean-squared displacement $\langle r^2(t)\rangle^{\frac{1}{2}}$, separated into 3 regimes of segmental dynamics based on MSD data and fitted in regimes I and II (black line). The blue line represents the prediction of the tube-reptation model. (b) The comparison of the same ratio obtained in this work with the FC data[24] as a function of the rescaled time.

on two reasons. First, both techniques provide the ratio $\frac{A^{\text{inter}}}{A^{\text{intra}}}$ based on different integral transformations of the total proton magnetic dipole-dipole correlation function. In the case of FC relaxometry, it is a weighted sum of Fourier transformations of the dipole-dipole correlation functions at the resonance and double resonance frequencies, whereas in the case of the spin echo method one deals with a convolution of the discussed dipole-dipole correlation function with time. This leads to a possible difference in the numerical coefficients and even in a functional behavior during the crossover between different regimes of macromolecular motion. However, it is emphasized that the ratio $\frac{A^{\text{inter}}}{A^{\text{intra}}}$ does not affect the MSD results, as according to Eq. (17), MSD depends only on the intermolecular part of the SE build-up function. Second, both methods can be subjects to additional disturbing effects at long times/low frequencies: FC in regime II, at frequencies on the order of 100 Hz, approaches the Redfield limit (problem mentioned in the Introduction), and SE and DC methods are affected by the spin non-equivalency and highly mobile impurities at high temperatures. Moreover, results provided by the multi-quantum (MQ) resonance method differ from the both sets of data presented here, yielding weaker isotope-dilution effects.[31] Therefore, FFC and time-domain (transverse-evolution) approaches such as MQ, HE, or SE have been observed before to provide different results for the inter/intra ratio. However, the significant uncertainties related to this ratio do not challenge the consistent MSD result. Generally, the relative contributions of intra- and intermolecular dipole-dipole interactions to the total proton dynamical correlation function will be studied in more details in the future, as it can provide a valuable insight on the segmental dynamics in a polymer melt.

CONCLUSION

In the present research, a novel approach to the investigation of segmental dynamics in entangled polymer melts, based on the formalism developed by the authors in previous works, was presented. It implies the use of the combination of pulse sequences $\left(\hat{P}_x^{\pi/2} - \tau - \hat{P}_y^{\pi/2}\right)$, $\left(\hat{P}_x^{\pi/2} - \tau - \hat{P}_x^{\pi/2}\right)$, and $\left(\hat{P}_x^{\pi/2} - \tau - \hat{P}_x^{\pi}\right)$ in isotopically diluted samples, and construction of the solid-echo build-up function I^{SE}, which allows one to extract the segmental mean-squared displacement in a melt and to study the dynamical proton dipole-dipole correlation function at the millisecond range, which is hardly accessible by other experimental methods. Using this method in combination with time-temperature superposition, MSD in a time range of 6 decades was obtained, yielding clear transitions of the power-law dependence between regimes I, II, and III in the frame of the tube-reptation model, with exponents being in good agreement with the values predicted by the theory. For the first time, the Rouse relaxation time τ_R for PEP 200k was measured, corresponding to the transition between regimes of the coherent and incoherent reptation. The tube diameter calculated from the obtained data, $d_t \approx 3.9$ nm, was in good agreement with literature data. The MSD findings were confirmed as well using an alternative method based on the dipolar-correlation effect on the Hahn echo (proposed by the authors in Ref. 41). However, the dependence of the relative intermolecular dipole-dipole interactions on the root mean-squared displacement was at variance with the predictions of the tube-reptation model for regimes II and III, whereas the result for regime I was in satisfactory agreement with the theory. For the more precise and detailed study of this phenomena, polyethylene oxide is being investigated, which has a simple structure and all the proton spins magnetically equivalent to each other, and the results of this work are going to be presented as well in the future contributions.

ACKNOWLEDGMENTS

Financial support from Deutsche Forschungsgemeinschaft (DFG) through Grant No. STA 511/13-1 is gratefully acknowledged. This work is also supported by a post-doc fellowship (M.H.) of the German Academic Exchange Service (DAAD). The authors thank D. Richter and L. Willner (Forschungszentrum Juelich, Germany) for providing the PEP samples. They also express their gratitude to R. Kimmich (Ulm University, Germany) and E. A. Roessler (University of Bayreuth, Germany) for fruitful discussions.

APPENDIX: CALCULATION OF S_1 SIGNAL

Consider a system described as in Ref. 35 by the following Hamiltonian:

$$\hat{H} = \hat{H}_s + \hat{H}_L + \hat{H}_{dd}^{sec}. \tag{A1}$$

In this expression, $\hat{H}_s = \sum_k \hbar\omega_0 \hat{I}_k^z$ is the Zeeman spin Hamiltonian describing the interaction of proton spins with the external magnetic field B_0, $\omega_0 = -\gamma B_0$ is the resonance frequency corresponding to that magnetic field, $\hat{H}_L$ is the Hamiltonian of the lattice degrees of freedom related to the motions of the macromolecules in space, and $\hat{H}_{dd}^{sec}$ is the secular part of the dipole-dipole interaction Hamiltonian, where only homonuclear interactions of ^{1}H nuclei are considered throughout the paper. The latter gives the main contribution to transverse relaxation at high frequencies and can be expressed in the standard way,

$$\hat{H}_{dd}^{sec} = \frac{1}{2}\sum_{k;l} A_{kl}\left(\hat{I}_k^z\hat{I}_l^z - \frac{1}{4}\left(\hat{I}_k^+\hat{I}_l^- + \hat{I}_k^-\hat{I}_l^+\right)\right), \tag{A2}$$

where for $i \neq j$

$$A_{kl} = \frac{\gamma^2\hbar^2}{r_{kl}^3}\left(1 - 3\cos^2(\theta_{kl})\right). \tag{A3}$$

Here γ denotes the gyromagnetic ratio of proton spins, k and l are the indices enumerating spins, r_{kl} is the distance between spins k and l, and θ_{kl} is the angle between the direction of B_0 and r_{kl}. $\hat{I}_k^z, \hat{I}_k^+ = \hat{I}_k^x + i\hat{I}_k^y, \hat{I}_k^- = \hat{I}_k^x - i\hat{I}_k^y$ are z-component, raising and lowering operators, respectively, of spin k, and $A_{ii} = 0$. For the better representation, the expression for $\hat{H}_{dd}^{sec}$ can be rewritten as follows:

$$\hat{H}_{dd}^{sec} = \frac{3}{4}\sum_{k;l} A_{kl}\hat{I}_k^z\hat{I}_l^z - \frac{1}{4}\sum_{k;l}\tilde{A}_{kl}\hat{\vec{I}}_k\cdot\hat{\vec{I}}_l. \tag{A4}$$

In Eq. (A4), $\hat{\vec{I}}_k\cdot\hat{\vec{I}}_l = \hat{I}_k^x\hat{I}_l^x + \hat{I}_k^y\hat{I}_l^y + \hat{I}_k^z\hat{I}_l^z$ and $\tilde{A}_{kl} = A_{kl} - 2J_{kl}$, where J_{kl} is the constant of an exchange interaction between spins k and l (Note that this is a correction of a misprint in

the corresponding expression in Ref. 35). The scalar part of (A4) is usually neglected for the sake of simplification of the calculations in the frame of the Anderson-Weiss approximation, used in the cases where incomplete motional narrowing conditions take place.[36] That term comprises the spin diffusion phenomenon due to the presence of the interspin flip-flop interactions. In Ref. 35, it was shown that taking into account the scalar term leads to a deviation from the standard Anderson-Weiss approach of less than 10% for times $t \leq 2T_2^{eff}$, where T_2^{eff} is the effective spin-spin relaxation time (time by which magnetization decays by e times) of a spin system governed by the Hamiltonian (A2), which means that in this time range neglecting the scalar term while for analyzing experimental data is acceptable.

Following the same formalism, consider the response of the spin system to the RF pulse sequence $(\hat{P}_x^{\pi/2} - \tau - \hat{P}_y^{\pi/2})$ — the so-called solid echo.

At the time origin, the state of the total (spin + lattice) system is described by the equilibrium density matrix,

$$\hat{\rho}^{eq} = \frac{1}{Z}\exp\left(-\beta\hat{H}\right) \cong \hat{\rho}_s^{eq}\hat{\rho}_L^{eq} = \frac{1}{Z_s}\exp\left(-\beta\hat{H}_s\right)\hat{\rho}_L^{eq} \cong \frac{1}{Z_s}\exp\left(I - \beta\hbar\omega_0\hat{I}_z\right)\hat{\rho}_L^{eq}. \quad \text{(A5)}$$

In this expression, $\beta = \frac{1}{k_B T}$ is the inverse temperature of the system, $\hat{\rho}_L^{eq}$ is the equilibrium density matrix of the lattice, $Z_s \cong (2I+1)^{N_s}$ is the statistical sum of the spin system in the high-temperature approximation, i.e., $\beta\hbar\omega_0 << 1$, which is valid with high accuracy at any temperature above ≈10 mK, N_s is the total number of spins in the system with the resonance frequency ω_0, and $\hat{I}_z = \sum_k \hat{I}_k^z$. After application of the first RF pulse, rotating the spins by an angle $\pi/2$ about the x axis, the equilibrium matrix turns into

$$\hat{\rho}_0 = \hat{P}_x^{\pi/2}\hat{\rho}^{eq} \equiv \exp\left(-i\frac{\pi}{2}\hat{I}_x\right)\hat{\rho}^{eq}\exp\left(i\frac{\pi}{2}\hat{I}_x\right) \cong \frac{1}{Z_s}\left(I + \beta\hbar\omega_0\hat{I}_y\right)\hat{\rho}_L^{eq}. \quad \text{(A6)}$$

The system now follows the free evolution determined by the Hamiltonian (A1) and the density matrix of the total system at time t is equal to

$$\hat{\rho}(t) = \hat{S}(t)\hat{\rho}_0 = \exp\left(-it\hat{L}_H\right)\hat{\rho}_0, \quad \text{(A7)}$$

where, for the purpose of abbreviation, the Liouville space formalism is used (see, for example, Ref. 13), i.e., $\hat{S}(t)$ is the superoperator of the evolution caused by the Hamiltonian $\hat{H} = \hat{H}_s + \hat{H}_L + \hat{H}_{dd}^{sec}$, which, by definition, is acting in accordance with the following rule:

$$\hat{S}(t)\hat{\rho}_0 = \exp\left(-i\hat{H}t\right)\hat{\rho}_0\exp\left(i\hat{H}t\right). \quad \text{(A8)}$$

$\hat{L}_H$ is the Liouville operator defined by the relation

$$\hat{L}_H\hat{\rho} = \frac{1}{\hbar}\left[\hat{H};\hat{\rho}\right]. \quad \text{(A9)}$$

Consequently, at time $t = \tau$, the second RF pulse $\hat{P}_y^{\pi/2}$ acts on the spin system and rotates the spin system by the angle $\frac{\pi}{2}$ about the y axis. Considering the situation when the experimentally measurable quantity is the y component of the total spin of the system, its value at time t can be calculated with the help of the statistical operator, yielding the following standard relation:

$$S_1(t) \equiv \left\langle \hat{I}_y(t)\right\rangle = Tr\left(\hat{I}_y\hat{\rho}(t)\right) \cong \frac{\beta\hbar\omega_0}{(2I+1)^{N_s}}Tr\left(\hat{I}_y\hat{S}(t-\tau)\hat{P}_y^{\pi/2}\hat{S}(\tau)\hat{I}_y\hat{\rho}_L^{eq}\right), \quad \text{(A10)}$$

where $Tr(\dots)$ is the trace operation over all the spin and lattice variables and $\hat{I}_y = \sum_k \hat{I}_k^y$.

Within the accuracy of the high-temperature approximation expression (A10) is exact. Its further evaluation demands approximations due to the presence of the multiparticle interaction term $\hat{H}_{dd}^{sec}$ given by expression (A2) in the total Hamiltonian (A1). Subsequently, the modified Anderson-Weiss approximation is used, details of which can be found in Ref. 35.

A first step of this approximation is based on the transition to the so-called interaction, or Dirac, representation. The main difference from usual standard schemes is contained in choosing the so-called "Zero Hamiltonian," which in the present case includes the scalar part of the Hamiltonian (A1), defined as

$$\hat{H}_0 = \hat{H}_s + \hat{H}_L - \frac{1}{4}\sum_{k;l}\tilde{A}_{kl}\hat{\tilde{I}}_k\cdot\hat{\tilde{I}}_l. \quad \text{(A11)}$$

Therefore in our case the role of perturbation is assumed by the following Hamiltonian:

$$\hat{H}_{dd}^{sec;zz} = \frac{3}{4}\sum_{k;l}A_{kl}\hat{I}_k^z\hat{I}_l^z. \quad \text{(A12)}$$

Expression (A10) can be rewritten as

$$S_1(t) = \frac{\beta\hbar\omega_0}{(2I+1)^{N_s}}Tr\left(\hat{I}_y\hat{S}_0(t)\hat{\tilde{S}}_{dd}^{\text{sec}}(t-\tau;\tau)\hat{S}_0^{-1}(\tau)\hat{P}_y^{\pi/2} \times \hat{S}_0(\tau)\hat{\tilde{S}}_{dd}^{\text{sec}}(\tau;0)\hat{I}_y\hat{\rho}_L^{eq}\right). \quad \text{(A13)}$$

Here, $\hat{S}_0(t) = \exp\left(-it\hat{L}_0\right)$ is the superoperator of evolution created by the Hamiltonian (A11), and

$$\hat{\tilde{S}}_{dd}^{\text{sec}}(t_2;t_1) = \hat{T}\exp\left\{-i\int_{t_1}^{t_2}\hat{\tilde{L}}_{dd}^{\text{sec};zz}(t')dt'\right\} \quad \text{(A14)}$$

is the superoperator of evolution created by the Hamiltonian (A12) in the interaction representation, where $\hat{T}$ means the usual Dyson time ordering operator.

Then, for the calculation with superoperator (A14), one can use the standard quantum statistical perturbation theory to (A14) truncating the series decomposition on terms having second order of magnitude with respect to $\int_{t_1}^{t_2}\hat{\tilde{L}}_{dd}^{\text{sec};zz}(t)$. Then contributions of higher orders of magnitude can be recovered using the second cumulant, i.e., the Anderson-Weiss, approximation for calculating the spin echo signal. For realization of this procedure, it is necessary to be able to calculate the time evolution of operators having the structure

$$\hat{S}_0^*(t)\hat{I}_k^z\hat{I}_l^z = \exp\left\{i\frac{\hat{H}_0}{\hbar}t\right\}\hat{I}_k^z\hat{I}_l^z\exp\left\{-i\frac{\hat{H}_0}{\hbar}t\right\}. \quad \text{(A15)}$$

In our case, the Zero Hamiltonian includes the scalar part of the spin-spin interactions and, due to that, the right part of expression (A15) cannot be calculated exactly. The approximation suggested in Ref. 35 consists of the right-hand side of operators having a structure similar to (A15) by its projection in the sense of Zwanzig-Mori; see, for example, Ref. 53,

$$\hat{S}_0^*(t)\hat{I}_k^z\hat{I}_l^z \approx \hat{P}_{kl}^{zz}\hat{S}_0^*(t)\hat{I}_k^z\hat{I}_l^z \equiv \hat{I}_k^z\hat{I}_l^z\frac{Tr(\hat{I}_k^z\hat{I}_l^z\hat{S}_0^*(t)\hat{I}_k^z\hat{I}_l^z\hat{\rho}_L^{eq})}{Tr_s(\hat{I}_k^z\hat{I}_l^z)^2} = \hat{I}_k^z\hat{I}_l^z P_{kl}^{fl}(t), \tag{A16}$$

where $Tr_s(\ldots)$ is the trace operation over all the spin variables.

Note that experimentally measurable quantities are time-dependent correlation functions having structures similar to (A13). They do not depend on the choice of the initial moment of time. The approximation (A16) obviously does not possess this feature; therefore, it should be applied with additional instructions to keep the discussed property. First of all, time-dependent correlation functions should be rewritten into "normal form," which means that the argument t_i of the spin operators as $\hat{S}_0^*(t_i)\hat{I}_k^z\hat{I}_l^z$ at the initial moment of time is zero. Then the approximation (A16) should be applied to these time-dependent correlation functions written in the "normal form." For instance, let us discuss how to calculate a quantity, which has the structure of the form $J(t_2;t_1) = Tr\left(\left(\hat{S}_0^*(t_i)\hat{I}_k^z\hat{I}_l^z\right)\hat{B}\left(\hat{S}_0^*(t_i)\hat{I}_k^z\hat{I}_l^z\right)\hat{\rho}_L^{eq}\right)$, where $\hat{B}$ is a time independent operator. Taking advantage of a translational invariance, we can represent it in the normal form as follows: $J(t_2;t_1) = Tr\left(\left(\hat{S}_0^*(t_2-t_1)\hat{I}_k^z\hat{I}_l^z\right)\hat{B}\hat{I}_k^z\hat{I}_l^z\hat{\rho}_L^{eq}\right)$. It is possible now to apply the approximation (A16) and obtain $J(t_2;t_1) = P_{kl}^{fl}(t_2-t_1)Tr\left(\hat{I}_k^z\hat{I}_l^z\hat{B}\hat{I}_k^z\hat{I}_l^z\hat{\rho}_L^{eq}\right)$. Here, $P_{kl}{}^{fl}$ can be considered as the probability for a given pair of spins with numbers k and l not to participate in flip-flop processes in the time interval t. For protons, which have a spin $I = \frac{1}{2}$ mutual flip-flop transitions between spins with numbers k and l do not give a contribution to the probability P_{kl}^{fl}. The expression for this probability was derived with the use of the standard Anderson-Weiss approximation in Ref. 35,

$$P_{kl}^{fl}(t) = \exp\left\{-\int_0^t d\tau\,(t-\tau)\frac{I(I+1)}{6\hbar^2}\sum_m\left(\left\langle\tilde{A}_{km}(\tau)\tilde{A}_{km}(0)\right\rangle_{eq} + \left\langle\tilde{A}_{lm}(\tau)\tilde{A}_{lm}(0)\right\rangle_{eq}\right)\right\}. \tag{A17}$$

Expression (A13) for the signal S_1 can be rewritten in the following form:

$$S_1(t) = \frac{\beta\hbar\omega_0}{(2I+1)^{N_s}}Tr\left(\left(\hat{S}_0(\tau)\left(\hat{\tilde{S}}_{dd}^{\sec}(t-\tau;\tau)\right)^{-1}\hat{S}_0^{-1}(t)\hat{I}_y\right)\hat{P}_y^{\pi/2} \times\hat{S}_0(\tau)\hat{\tilde{S}}_{dd}^{\sec}(\tau;0)\hat{I}_y\hat{\rho}_L^{eq}\right). \tag{A18}$$

Employing the approximation (A16), the action of evolution superoperators on the spin variables $\hat{S}_0(\tau)\left(\hat{\tilde{S}}_{dd}^{\sec}(t-\tau;\tau)\right)^{-1}\hat{S}_0^{-1}(t)\hat{I}_y$ and $\hat{S}_0(\tau)\hat{\tilde{S}}_{dd}^{\sec}(\tau;0)\hat{I}_y$ can be calculated exactly. Then, using properties of the spin $I = \frac{1}{2}$, symmetry arguments like the isotropy of the system, considering motions of lattice variables classically, after somewhat bulky quantum statistical calculations, which were described in details in Ref. 35, one obtains the following result:

$$S_1(t) = \frac{\beta\hbar\omega_0}{4}\sum_{k;s}\left\langle\cos(\tilde{\varphi}_s(t-\tau))\cos(\varphi_k(\tau)) \times\left(\delta_{ks}+4\frac{\partial^2}{\partial\tilde{\varphi}_{ks}^d\partial\varphi_{ks}^d}\right)\prod_m\cos\left(\frac{\tilde{\varphi}_{sm}^d(t-\tau)}{2}\right) \times\cos\left(\frac{\varphi_{km}^d(\tau)}{2}\right)\right\rangle, \tag{A19}$$

where

$$\varphi_{kl}^d(\tau) = \frac{3\gamma^2\hbar}{2}\int_0^\tau dt_1\frac{1-3\cos^2(\theta_{kl}(t_1))}{r_{kl}^3(t_1)}P_{kl}^{fl}(t_1), \tag{A20}$$

$$\tilde{\varphi}_{km}^d(t-\tau) = \frac{3\gamma^2\hbar}{2}\int_\tau^t dt_1\frac{1-3\cos^2(\theta_{km}(t_1))}{r_{km}^3(t_1)}P_{km}^{fl}(t_1), \tag{A21}$$

the phases $\varphi_k(\tau) = \omega_k\cdot\tau$, and $\tilde{\varphi}_s(t-\tau) = \omega_s\cdot(t-\tau)$ are connected with either chemical shift differences of different protons or different Larmor frequencies caused by an external magnetic field gradient, the latter being assumed small enough for neglecting diffusion effects. The bracket $\langle\ldots\rangle$ denotes, as usual, the equilibrium averaging over lattice variables. The quantities $\varphi_{km}^d(\tau)$ and $\tilde{\varphi}_{sm}^d(t-\tau)$, where $\varphi_{ii}^d(\tau) = \tilde{\varphi}_{jj}^d(t-\tau) = 0$, are related to rotations of proton spins in local dipolar fields after the first and the second RF pulses, respectively, and contain information about polymer segments dynamics through time dependence of the factors $\frac{1-3\cos^2(\theta_{km}(t_1))}{r_{km}^3(t_1)}$ inside integrals at the right-hand side of expressions (A20) and (A21). In the course of formal partial differentiations over $\varphi_{km}^d(\tau)$ and $\tilde{\varphi}_{sm}^d(t-\tau)$, these quantities should be considered as independent variables. After that, it is necessary to use the expressions (A20) and (A21) and then to make a statistical averaging. Due to the factors $\cos(\tilde{\varphi}_s(t-\tau))\cos(\varphi_k(\tau))$ and $\cos\left(\frac{\tilde{\varphi}_{sm}^d(t-\tau)}{2}\right)\cos\left(\frac{\varphi_{km}^d(\tau)}{2}\right)$ the signal $S_1(t)$ has a maximum, i.e., an echo, at time $t = 2\tau$. Note also, that the echo can be observed even in the situations, which are actually rather difficult to realize experimentally, when the phases $\varphi_k(\tau)$ and $\tilde{\varphi}_k(t-\tau)$ are very small, but motion of spins before and after the second RF pulse are correlated due to the factor $\cos\left(\frac{\tilde{\varphi}_{sm}^d(t-\tau)}{2}\right)\cos\left(\frac{\varphi_{km}^d(\tau)}{2}\right)$.

The signals $S_2(t)$ and $S_3(t)$ can be calculated analogously,

$$S_2(t) = \frac{\beta\hbar\omega_0}{4}\sum_{k;s}\left\langle\sin(\tilde{\varphi}_s(t-\tau))\sin(\varphi_k(\tau)) \times\left(\delta_{ks}+4(1-\delta_{ks})\frac{\partial^2}{\partial\tilde{\varphi}_{ks}^d\partial\varphi_{ks}^d}\right)\prod_m \times\cos\left(\frac{\tilde{\varphi}_{sm}^d(t-\tau)}{2}\right)\cos\left(\frac{\varphi_{km}^d(\tau)}{2}\right)\right\rangle, \tag{A22}$$

$$S_3(t) = \frac{\beta\hbar\omega_0}{4}\sum_k \left\langle \cos\left(\tilde{\varphi}_k(t-\tau) - \varphi_k(\tau)\right) \times \prod_m \cos\left(\frac{1}{2}\left(\tilde{\varphi}^d_{km}(t-\tau) + \varphi^d_{km}(\tau)\right)\right)\right\rangle. \quad \text{(A23)}$$

The most important difference between the Hahn echo, signal S_3, and the two variants of the solid echo, signal S_1, which is usually named the solid echo, and signal S_2, occurs in the factor $\cos\left(\frac{1}{2}\left(\tilde{\varphi}^d_{km}(t-\tau) + \varphi^d_{km}(\tau)\right)\right)$, which considers the influence of the local dipolar fields on the spin evolution to be additive, as this expression contains the sum of phases $\frac{1}{2}\left(\tilde{\varphi}^d_{km}(t-\tau) + \varphi^d_{km}(\tau)\right)$, where the factor $\frac{1}{2}$ reflects the fact that spin $I = \frac{1}{2}$ is treated. Note that at time $t = 2\tau$ Eq. (A23) is equivalent to the expression derived in the same way for the FID signal in Ref. 35.

Now consider the sum of two echo signals S_1 and S_2, which were calculated before,

$$S_{12}(t) \equiv S_1(t) + S_2(t) = \frac{\beta\hbar\omega_0}{4}\sum_{k;s}\left\langle \cos\left(\tilde{\varphi}_s(t-\tau) - \varphi_k(\tau)\right) \times\left(\delta_{ks} + 4\frac{\partial^2}{\partial\tilde{\varphi}^d_{ks}\partial\varphi^d_{ks}}\right)\prod_m \cos\left(\frac{\tilde{\varphi}^d_{sm}(t-\tau)}{2}\right) \times \cos\left(\frac{\varphi^d_{km}(\tau)}{2}\right)\right\rangle. \quad \text{(A24)}$$

This sum has the same echo forming factor $\cos\left(\tilde{\varphi}_k(t-\tau) - \varphi_k(\tau)\right)$ as the Hahn echo (A23). Using this feature and the fact that all the discussed signals have a maximal value at time $t = 2\tau$, the normalized function, which reflects the difference between the solid and Hahn echoes, $I^{SE}(t)$ is defined as

$$I^{SE}(t) \equiv \frac{S_{12}(t) - S_3(t)}{S_{12}(t)}. \quad \text{(A25)}$$

At time $t = 2\tau$, when one can neglect the effects caused by the difference of chemical shifts between different spins, the value $\cos\left(\tilde{\varphi}_k(t-\tau) - \varphi_k(\tau)\right) \approx 1$ and, in particular for polymer melts with large molecular masses, the dependence of each contribution inside the sums in expressions (A7) and (A8) on the spin number k is very weak, i.e., they are equal to each other. Therefore, one can derive from (A23)–(A25),

$$I^{SE}(t) = 1 - \frac{\sum_k\left\langle\prod_m \cos\left(\frac{1}{2}\left(\tilde{\varphi}^d_{km}(\tau) + \varphi^d_{km}(\tau)\right)\right)\right\rangle}{\sum_{k;s}\left\langle\left(\delta_{ks} + 4\frac{\partial^2}{\partial\tilde{\varphi}^d_{ks}\partial\varphi^d_{ks}}\right)\prod_m \cos\left(\frac{\tilde{\varphi}^d_{sm}(\tau)}{2}\right)\cos\left(\frac{\varphi^d_{km}(\tau)}{2}\right)\right\rangle}. \quad \text{(A26)}$$

A many-spin generalization of the $\beta(2\tau;\tau)$ function, described in Ref. 45, can be obtained from the expression (A25) as well if one replaces $S_{12}(t)$ in the denominator with its initial value $S_{12}(2\tau = 0;\ \tau = 0)$, which is actually not straightforward to determine experimentally.

Then, employing the following approximation for the cosine function in (A26):

$$\cos(x) = 1 - \frac{1}{2}x^2 + \ldots \cong \exp\left\{-\frac{1}{2}x^2\right\}, \quad \text{(A27)}$$

expression (A25) can be evaluated as

$$I^{SE}(t) = 1 - \frac{\sum_k \exp\left\{-\frac{1}{8}\sum_m\left\langle\left(\tilde{\varphi}^d_{km}(\tau) + \varphi^d_{km}(\tau)\right)^2\right\rangle\right\}}{\sum_k \exp\left\{-\frac{1}{8}\sum_m\left\langle\left(\tilde{\varphi}^d_{km}(\tau) - \varphi^d_{km}(\tau)\right)\right\rangle\right\}}. \quad \text{(A28)}$$

[1] V. A. Kargin and G. L. Slonimskii, J. Fizhimii (USSR) **23**, 563 (1949).
[2] P. J. Rouse, J. Chem. Phys. **21**, 1272 (1953).
[3] N. Fatkullin, R. Kimmich, and H. W. Weber, Phys. Rev. E **47**(6), 4600 (1993).
[4] N. Fatkullin and R. Kimmich, J. Chem. Phys. **101**(1), 822 (1994).
[5] S. F. Edwards, Proc. Phys. Soc. **92**, 9 (1967).
[6] P. G. de Gennes, J. Chem. Phys. **55**, 572 (1971).
[7] M. Doi and S. F. Edwards, J. Chem. Soc., Faraday Trans. 2 **74**, 1789 (1978).
[8] M. Doi and S. F. Edwards, *The Theory of Polymer Dynamics* (Clarendon, Oxford, 1986).
[9] K. S. Schweizer, J. Chem. Phys. **91**, 5802 (1989).
[10] K. S. Schweizer, J. Chem. Phys. **91**, 5822 (1989).
[11] K. S. Schweizer, Phys. Scr. **T49A**, 99 (1993).
[12] A. Abragam, *The Principles of Nuclear Magnetism* (Clarendon, Oxford, 1961).
[13] C. P. Slichter, *Principles of Magnetic Resonance*, 3rd ed. (Springer-Verlag, Berlin, Heidelberg, New York, 1990).
[14] R. Kimmich and N. Fatkullin, Adv. Polym. Sci. **170**, 1 (2004).
[15] R. Kimmich, N. Fatkullin, R.-O. Seitter, and K. Gille, J. Chem. Phys. **108**, 2173 (1998).
[16] M. Kehr, N. Fatkullin, and R. Kimmich, J. Chem. Phys. **126**, 094903 (2007).
[17] M. Kehr, N. Fatkullin, and R. Kimmich, J. Chem. Phys. **127**, 084911 (2007).
[18] R. Kimmich and N. Fatkullin, Prog. Nucl. Magn. Reson. Spectrosc. **101**, 18 (2017).
[19] E. A. Rössler, S. Stapf, and N. Fatkullin, Curr. Opin. Colloid Interface Sci. **18**(3), 173 (2013).
[20] S. Kariyo, A. Brodin, C. Gainaru, A. Herrmann, J. Hintermeyer, H. Schick, V. N. Novikov, and E. A. Rössler, Macromolecules **41**, 5322 (2008).
[21] S. Kariyo, A. Herrmann, C. Gainaru, H. Schick, A. Brodin, V. N. Novikov, and E. A. Rössler, Macromolecules **41**, 5313 (2008).
[22] A. Herrmann, B. Kresse, J. Gmeiner, A. F. Privalov, D. Kruk, F. Fujara, and E. A. Rössler, Macromolecules **45**, 6516 (2012).
[23] M. Hofmann, B. Kresse, A. F. Privalov, L. Heymann, L. Willner, N. Aksel, N. Fatkullin, F. Fujara, and E. A. Rössler, Macromolecules **49**(20), 7945 (2016).
[24] M. Hofmann, B. Kresse, L. Heymann, A. F. Privalov, L. Willner, N. Fatkullin, N. Aksel, F. Fujara, and E. A. Rössler, Macromolecules **49**(22), 8622 (2016).
[25] B. Kresse, M. Hofmann, A. F. Privalov, N. Fatkullin, F. Fujara, and E. A. Rössler, Macromolecules **48**(13), 4491 (2015).
[26] E. Fischer, R. Kimmich, N. Fatkullin, and G. Yatsenko, Phys. Rev. E **62**, 775 (2000).
[27] D. Richter, M. Monkenbusch, A. Arbe, and J. Colmenero, Adv. Polym. Sci. **174**, 1 (2005).
[28] A. Wischnewski, M. Monkenbusch, L. Willner, D. Richter, and G. Kali, Phys. Rev. Lett. **90**(5), 58302 (2003).
[29] D. Richter, R. Butera, L. J. Fetters, J. S. Huang, B. Farago, and B. Ewen, Macromolecules **25**(23), 6156 (1992).
[30] R. Graf, A. Heuer, and H. W. Spiess, Phys. Rev. Lett. **80**, 5738 (1998).
[31] F. Furtado, J. Damron, M.-L. Trutschel, C. Franz, K. Schröter, R. C. Ball, K. Saalwaechter, and D. Panja, Macromolecules **47**(1), 256 (2014).
[32] F. Vaca Chávez and K. Saalwächter, Phys. Rev. Lett. **104**(19), 198305 (2010).
[33] F. Vaca Chávez and K. Saalwächter, Macromolecules **44**(6), 1549 (2011).
[34] N. Fatkullin, C. Mattea, and S. Stapf, J. Chem. Phys. **139**, 194905 (2013).
[35] N. Fatkullin, A. Gubaidullin, C. Mattea, and S. Stapf, J. Chem. Phys. **137**, 224907 (2012).
[36] P. W. Anderson and P. R. Weiss, Rev. Mod. Phys. **25**, 269 (1953).
[37] J. P. Cohen-Addad and M. Domard, J. Chem. Phys. **75**(8), 4107 (1981).
[38] M. G. Brereton, Macromolecules **22**(9), 3667 (1989).
[39] M. G. Brereton, Macromolecules **23**, 1119 (1990).
[40] R. Kimmich, E. Fischer, P. Callaghan, and N. Fatkullin, J. Magn. Reson., Ser. A **117**, 53 (1995).
[41] A. Lozovoi, C. Mattea, A. Herrmann, E. A. Rössler, S. Stapf, and N. Fatkullin, J. Chem. Phys. **144**(24), 241101 (2016).

[42]J. P. Cohen-Addad and R. Vogin, Phys. Rev. Lett. **33**(16), 940 (1974).
[43]J. Collignon, H. Sillescu, and H. W. Spiess, Colloid Polym. Sci. **259**(2), 220 (1981).
[44]P. T. Callaghan and E. T. Samulski, Macromolecules **30**(1), 113 (1997).
[45]R. C. Ball, P. T. Callaghan, and E. T. Samulski, J. Chem. Phys. **106**, 7352 (1997).
[46]J. P. Cohen-Addad, Prog. NMR Spectrosc. **25**, 1 (1993).
[47]J. T. Gotro and W. W. Graessley, Macromolecules **17**, 2767 (1984).
[48]L. J. Fetters, D. J. Lohse, D. Richter, T. A. Witten, and A. Zirkel, Macromolecules **27**(17), 4639 (1994).
[49]M. Flämig, M. Becher, M. Hofmann, T. Körber, B. Kresse, A. F. Privalov, L. Willner, D. Kruk, F. Fujara, and E. A. Rössler, J. Phys. Chem. B **120**, 7754 (2016).
[50]B. Schmidtke, M. Hofmann, A. Lichtinger, and E. A. Rössler, Macromolecules **48**(9), 3005 (2015).
[51]K. Halbach, Nucl. Instrum. Methods **169**(1), 1 (1980).
[52]N. Fatkullin, A. Gubaidullin, and S. Stapf, J. Chem. Phys. **132**, 094903 (2010).
[53]M. Mehring, *Principles of High Resolution NMR in Solids*, 2nd ed. (Springer-Verlag, Berlin, Heidelberg, New York, 1983).